

NANOSTRUCTURED SUPERCONDUCTOR/ FERROMAGNET BILAYERS

M. LANGE, M. J. VAN BAEL, L. VAN LOOK, S. RAEDTS,
V. V. MOSHCHALOV and Y. BRUYNSERAEDE
*Laboratorium voor Vaste-Stoffysica en Magnetisme
Katholieke Universiteit Leuven
Celestijnenlaan 200D
B-3001 Leuven Belgium*

1. Introduction

Magnetic field can penetrate type-II superconductors in the form of vortices. Each vortex carries a magnetic flux that is an integer multiple of the flux quantum ϕ_0 . The pinning properties of the vortices determine the magnitude of the critical current density (j_c) and the magnetisation (M) of the superconductor. Advances in nanolithography have allowed the fabrication of superconducting thin films with artificial pinning arrays like antidot lattices [1, 2] or lattices of magnetic dots [3, 4, 5, 6, 7]. These pinning centres give rise to a huge enhancement of j_c and M and can be used to stabilize new vortex phases like multiquanta and composite vortex lattices [2]. Pronounced commensurability effects between the vortex lattice and the array of pinning sites can be observed as peaks or cusps in $j_c(H)$ and $M(H)$ at specific values of the perpendicularly applied magnetic field H . We report on two different types of magnetic pinning centres with out-of-plane magnetisation. In the first type of sample, the Pb film is deposited on a square array of Co/Pt multilayer *dots*, the second system consists of a Pb film that is grown on a Co/Pt multilayer containing a regular array of *antidots*. In both systems, we will investigate how the direction of the magnetic moments in the Co/Pt multilayer influences the flux pinning in the superconducting film. These studies enable us to elucidate the pinning potential that the magnetic nanostructures impose in the superconducting film.

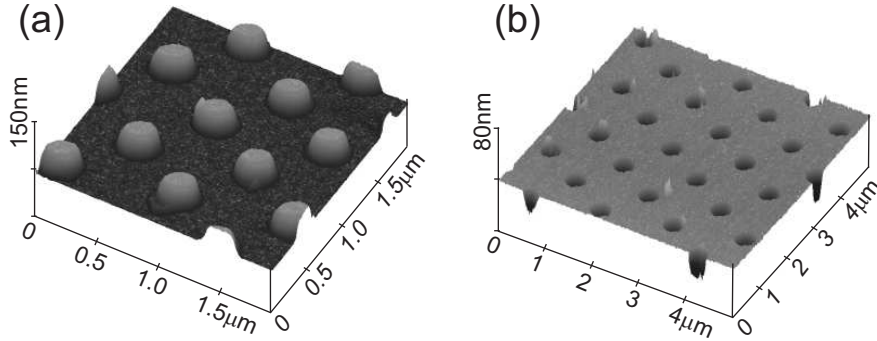


Figure 1. AFM micrographs of a square array of magnetic Co/Pt dots (a) and Co/Pt antidots (b). The dots $(\text{Pt}(6.4 \text{ nm})/[\text{Co}(0.5 \text{ nm})/\text{Pt}(1.6 \text{ nm})]_{10})$ have a diameter of $0.26 \mu\text{m}$, the lattice period amounts to $0.6 \mu\text{m}$. The antidot array (period $1 \mu\text{m}$) is defined by square holes with a side length of $0.37 \mu\text{m}$ in a $\text{Pt}(2.8 \text{ nm})/[\text{Co}(0.4 \text{ nm})/\text{Pt}(1.0 \text{ nm})]_{10}$ multilayer.

2. Sample preparation and characterization

2.1. PREPARATION

All samples were prepared on Si substrates with an amorphous SiO_2 top layer. For preparation of the Co/Pt dots, electron-beam lithography is used to define an array of holes in a resist layer on the substrate. For fabrication of the magnetic antidots, the resist on the substrate is pre-defined as an array of dots. A Co/Pt multilayer is then evaporated in the resist mask with a deposition rate of 0.01 nm/s for both Co and Pt at a working pressure of 10^{-8} Torr . Finally the resist is removed in a lift-off procedure, leaving an array of dots or antidots on the substrate. Figure 1 shows two atomic force microscopy (AFM) images of an array of Co/Pt dots and Co/Pt antidots. Two Co/Pt dot samples were studied consisting of $[\text{Co}(0.5 \text{ nm})/\text{Pt}(1.6 \text{ nm})]_{10}$ on a 6.4 nm Pt base layer and $[\text{Co}(0.4 \text{ nm})/\text{Pt}(0.9 \text{ nm})]_{10}$ on a 2.5 nm Pt base layer. For both dot arrays, the square lattice period is $0.6 \mu\text{m}$ and the dots have the shape of a disk with $0.26 \mu\text{m}$ diameter.

The antidot sample was made from a Co/Pt multilayer consisting of a 2.8 nm Pt base layer and $[\text{Co}(0.4 \text{ nm})/\text{Pt}(1.0 \text{ nm})]_{10}$. The antidots have square shape with rounded corners, their side length amounts to $0.37 \mu\text{m}$, and they are arranged in a square array with period $1 \mu\text{m}$.

After the magnetic properties of the samples were characterized, they were covered with a Ge/Pb/Ge trilayer by electron-beam evaporation at a working pressure of 10^{-8} Torr . In order to prevent the direct influence of the proximity effects between Pb and Co/Pt, a 10 nm insulating amorphous Ge layer is deposited first with a growth rate of 0.2 nm/s , then the 50 nm

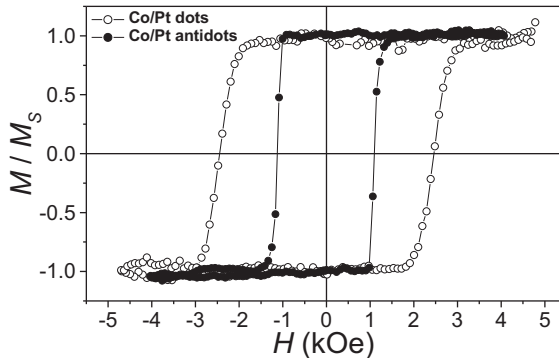


Figure 2. MOKE hysteresis loops of the Pt(2.5 nm)/[Co(0.4 nm)/Pt(0.9 nm)]₁₀ dot array and the array of antidots in a Pt(2.8 nm)/[Co(0.4 nm)/Pt(1.0 nm)]₁₀ multilayer (Co/Pt antidots) measured at room temperature and with H applied perpendicular to the sample surface.

Pb film is evaporated at a substrate temperature of 77 K with a growth rate of 1.0 nm/s and finally, the sample is covered with a 30 nm Ge layer for protection against oxidation. AFM images reveal that smooth Pb layers are obtained, which completely cover the dots and antidots. The critical temperature of the superconducting Pb films is $T_c = 7.20$ K.

2.2. MAGNETIC CHARACTERIZATION

The easy axis of magnetisation in Co/Pt multilayers prepared with correct film thicknesses lies perpendicular to the sample surface [8]. The out-of-plane anisotropy in our samples is confirmed by magnetisation measurements using the magneto-optical Kerr effect (MOKE) before deposition of the Ge/Pb/Ge trilayer. Figure 2 shows MOKE hysteresis loops of the Pt(2.5 nm)/[Co(0.4 nm)/Pt(0.9 nm)]₁₀ dot array and the Co/Pt antidot array in a perpendicularly applied field H . A 100 % remanence is observed for both samples with coercive fields of $H_c = 1.1$ kOe for the antidots and $H_c = 2.5$ kOe for the dots. This difference in H_c can be explained by the larger demagnetisation factors of the Co/Pt antidots compared to the dots. The domain structure of the samples is investigated by magnetic force microscopy (MFM). The MFM images in figure 3 show the dots in three different remanent states, after demagnetisation in a perpendicular field oscillating around zero with decreasing amplitude (a), after magnetisation in a large negative field of $H = -10$ kOe (b), and after magnetisation in a large positive field of $H = +10$ kOe (c). After demagnetisation, all dots produce a uniform dark or bright MFM signal, indicating a single domain

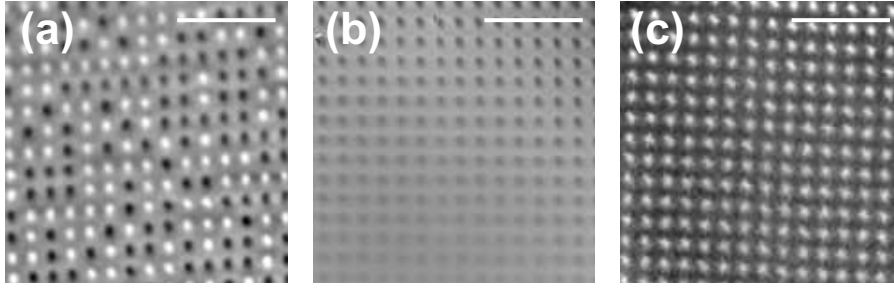


Figure 3. MFM images in zero field of a square array (period $0.6 \mu\text{m}$) of Pt(2.5 nm)/[Co(0.4 nm)/Pt(0.9 nm)]₁₀ dots (a) after out-of-plane demagnetisation; (b) and (c) in the remanent state after magnetisation perpendicular to the film plane in a -10 kOe and +10 kOe field, respectively. The white bar in all images corresponds to a length of $3 \mu\text{m}$.

state with the magnetic moments m either pointing up ($m > 0$) producing a bright signal, or pointing down ($m < 0$), giving rise to a dark signal. The average magnetic moment $\langle m \rangle$ is zero in this state. The MFM images in figure 3b and figure 3c confirm the 100 % magnetic remanence, since after magnetisation all dots produce a dark signal after saturation in $H < 0$ (figure 3b, $m < 0$), or they occur as bright spots after saturation in $H > 0$ (figure 3c, $m > 0$). Drift effects of the MFM tip during the scan cause the weaker signal of the dots at the bottom of figure 3b.

MFM measurements were also carried out on the Co/Pt antidot array, shown in figure 4. After demagnetisation, a band domain structure in the sample is clearly visible. The domains are observed as either bright or dark contrast, which can be associated with m either pointing up or down. The contrast appearing at the antidots themselves as white/black objects is possibly due to tip effects because of the topography. The remanent states are shown in the insets (a) and (b) of figure 4, and were obtained after magnetising the sample in fields of $H = +10 \text{ kOe}$ and $H = -10 \text{ kOe}$, respectively. In the inset (a), bright spots are observed at the position of the antidots which appear due to the mutually opposite direction of the stray field above the Co/Pt multilayer and above the antidots. If the Co/Pt multilayer is magnetised in the opposite direction, see figure 4 inset (b), the spots have a dark contrast due to the reversed polarity of the magnetic stray field.

3. Flux pinning experiments

In all flux pinning experiments, both the magnetic moments m of the Co/Pt multilayer and the applied field H are perpendicular to the sample surface. This leads to interesting magnetic interactions between the magnetic

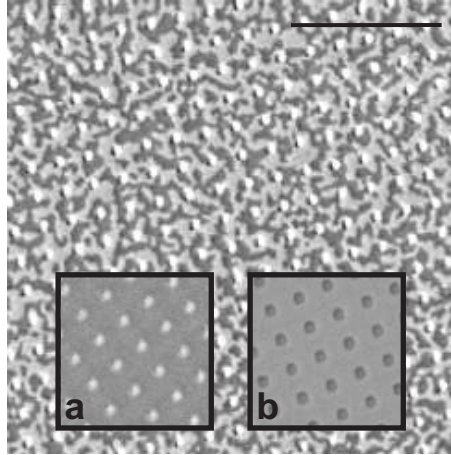


Figure 4. MFM image ($15 \mu\text{m} \times 15 \mu\text{m}$) in $H = 0$ of the square array of Co/Pt antidots after out-of-plane demagnetisation; the insets labeled by a and b show the remanent states after magnetisation perpendicular to the film plane in a +10 kOe and -10 kOe field, respectively. The black bar at the top of the image corresponds to a length of $5 \mu\text{m}$.

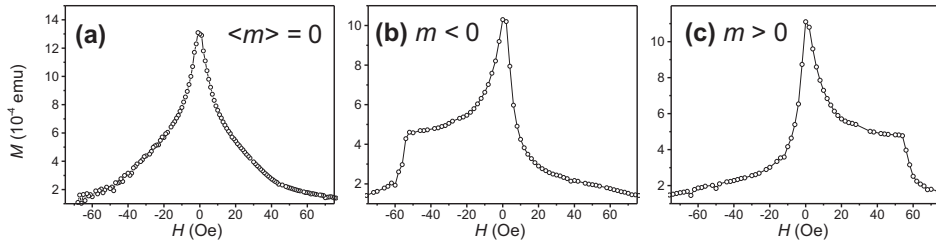


Figure 5. Upper half of the magnetisation loops $M(H)$ measured at $T = 6.61 \text{ K}$ of a 50 nm Pb film on the square array of $\text{Pt}(2.5 \text{ nm})/[\text{Co}(0.4 \text{ nm})/\text{Pt}(0.9 \text{ nm})]_{10}$ dots after demagnetising the dots perpendicular to the substrate (a); after magnetising the dots perpendicular to the substrate in -10 kOe (b) and +10 kOe (c).

nanostructures and flux lines, depending on the mutual orientation of m and H .

3.1. PINNING PROPERTIES OF MAGNETIC DOTS

The pinning properties were studied by SQUID magnetisation measurements $M(H)$. Figure 5 shows the upper branches of the magnetisation curves of the Pb film for $\langle m \rangle = 0$, $m < 0$ and $m > 0$. These three magnetic states correspond to the MFM images presented in figures 3a, b, and c, respectively. During the measurements, the magnetic state of the Co/Pt dots is preserved because H is always much smaller than the coercive field H_c

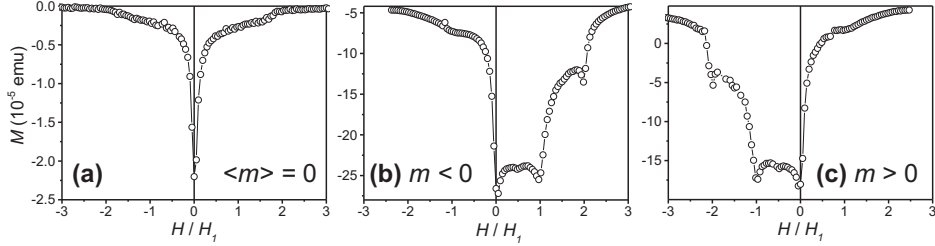


Figure 6. Lower half of the magnetisation loops $M(H/H_1)$ measured at $T = 7.05$ K of a 50 nm Pb film on top of the antidot array (a) after demagnetisation of the sample perpendicular to the substrate; (b) and (c) after magnetising the sample perpendicular to the substrate in -10 kOe and +10 kOe.

of the Co/Pt dots. The most obvious feature of figures 5b and c is the *clear asymmetry of the $M(H)$ curves with respect to the sign of the applied field*. A matching effect at the first matching field $H_1 = \phi_0/(600\text{nm})^2 = 57.4$ Oe and an enhancement of M are observed for aligned H and m , whereas no matching effects and a smaller M can be seen when H and m have opposite polarity. At H_1 , the field generates exactly one flux quantum ϕ_0 per unit cell of the dot array. The same asymmetry occurs in the lower branches of the $M(H)$ curves (not shown). The results presented in figures 5b and c indicate that the pinning force of the dots is much stronger when m and H have the same polarity.

The $M(H)$ curve for the dot array in the demagnetised state can be seen in figure 5a. No asymmetry and no matching effects appear for this magnetic state.

3.2. PINNING PROPERTIES OF MAGNETIC ANTIDOTS

The lower branches of the $M(H)$ curves of the Pb film on top of the Co/Pt multilayer with a square array of antidots is shown in figure 6 for the three different magnetic states (a) $\langle m \rangle = 0$, (b) $m < 0$ and (c) $m > 0$. The field axes were normalized to the first matching field $H_1 = \phi_0/(1\mu\text{m})^2 = 20.67$ Oe. Also for this sample, a strong asymmetry can be seen in the $M(H)$ curves presented in figures 6b and c. When H and m have the opposite polarity, a larger M and clear matching effects are observed at $H/H_1 = 1/2, 1$ and 2 for $m < 0$ and at $H/H_1 = -1/2, -1$ and -2 for $m > 0$, whereas for the same polarity of H and m , a smaller value of M is obtained and only weak deviations from the smooth curves are visible at $H/H_1 = -1$ for $m < 0$ and at $H/H_1 = 1$ for $m > 0$. In the $\langle m \rangle = 0$ state the $M(H)$ curve has a symmetric shape with respect to H . The magnitude of M is significantly smaller than in the magnetised states.

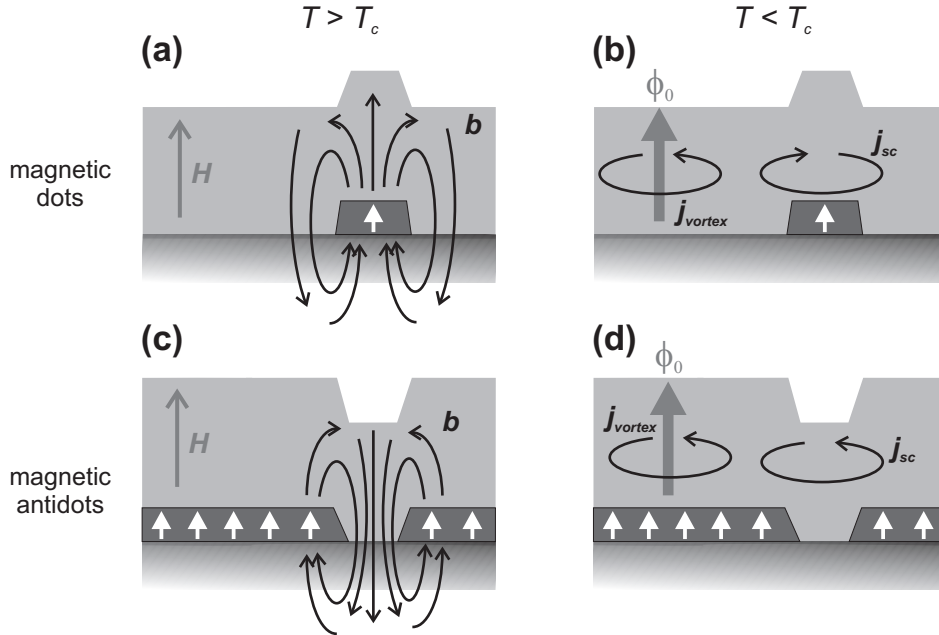


Figure 7. Schematic drawing to illustrate the behaviour of supercurrents j_{sc} and the stray field b of the magnetic nanostructures in the $m > 0$ state (a) above T_c for the magnetic dots, (b) below T_c for the magnetic dots (c) above T_c for the magnetic antidots, and (d) below T_c for the magnetic antidots. Above T_c , b can penetrate the Pb film without inducing supercurrents. Below T_c , b induces supercurrents j_{sc} , which interact with the supercurrents j_{vortex} around vortices that are generated by an applied field.

4. Discussion

We will now discuss the flux pinning potential that is created in the superconducting film by the magnetic nanostructures. A lot of different terms contribute to this potential: non-magnetic contributions like the corrugated surface of the Pb film as well as magnetic ones like the high magnetic permeability of the ferromagnet [3], the direction and magnitude of the magnetic moment [4, 5], the local stray field of the ferromagnet [6], and supercurrents induced by the local stray field [7]. Because of the asymmetry of the magnetisation curves, the dominating contribution must be a vector interaction, depending on the mutual orientation of H and m .

We will show that the experiments can be consistently explained by considering the interaction between flux lines and the supercurrents induced by the stray field of the magnetic nanostructures in the superconductor. Suppose that the sample is magnetised in a large positive field, resulting in a perpendicular component of the stray field that has a positive value above the dots (see figure 7a). Because of fluxoid quantization, this stray field can

only penetrate the superconductor in integer multiples of ϕ_0 below T_c . We assume that the stray field above the dots is not large enough to induce non-zero fluxoids in the superconductor. This means that the supercurrents j_{sc} that are generated by the stray field will try to screen the field from the interior of the superconductor. As a result j_{sc} will have a right-handed sense of rotation above the dots (see figure 7b). In a positive applied field the supercurrents around the vortices j_{vortex} have the opposite sense of rotation as j_{sc} . Consequently the vortices are attracted to the dots, resulting in the pronounced matching effect when m and H are aligned. On the other hand, flux lines that are generated by a negative applied field will be repelled from the dots because j_{vortex} has the same sense of rotation as j_{sc} . The flux lines will occupy the interstitial positions between the dots where they are weaker pinned. This causes the absence of matching effects when H and m have opposite polarity.

In the demagnetised state, the dots with $m > 0$ and $m < 0$ are randomly distributed over the square array. As a result, the pinning potential landscape is not periodic anymore and the pinning force is the same for negative and positive H . The lack of periodicity of the pinning potential is reflected by the symmetric shape of the $M(H)$ curve shown in figure 5(a).

The stray field of the magnetic antidots in the $m > 0$ state has opposite polarity compared to the magnetic dots in the $m > 0$ state (compare figures 7a and c). Therefore, assuming that also the magnetic antidots do not induce any fluxoids in the superconductor, j_{sc} above the antidots have opposite sense of rotation as j_{sc} above the dots, compare figure 7b with figure 7d. Consequently the magnetic antidots have opposite flux pinning properties as the magnetic dots and pronounced matching effects appear when H and m have opposite polarity. In the $\langle m \rangle = 0$ state, magnetic domains with m either pointing up or down are present in the sample (see figure 4). From the MFM image one can see that these domains are randomly distributed. This means that the stray field of the sample does not reflect the periodicity of the antidot array as in the $m > 0$ and the $m < 0$ state, resulting in the absence of matching effects and the symmetric $M(H)$ curve shown in figure 6a.

5. Conclusions

We have studied the pinning properties of a type-II superconducting film on top of two different types of *magnetic* artificial pinning centres. Such kind of pinning centres provides a strong pinning potential for the flux lines, yielding pronounced asymmetric $M(H)$ magnetisation curves for perpendicularly magnetised samples. This opens the opportunity to tune the

properties of a superconductor by switching between the magnetic states of the ferromagnetic nanostructures.

Acknowledgements

The authors thank R. Jonckheere (IMEC vzw), K. Temst and G. Güntherodt for help with sample preparation, D. Buntinx for MFM measurements and J. Swerts for MOKE measurements. This work is supported by the Belgian Inter-University Attraction Poles (IUAP) and Flemish Concerted Research Actions (GOA) programs, by the ESF "VORTEX" program and by the Fund for Scientific Research-Flanders (FWO). MJVB is a post-doctoral research fellow of the FWO.

References

1. Moshchalkov, V. V. *et al.* (1999), *Handbook of Nanostructured Materials and Nanotechnology*, Vol. 3, Chapter 9, edited by H. S. Nalwa, Academic Press, San Diego.
2. Baert M. *et al.* (1995) Composite flux-line lattices stabilized in superconducting films by a regular array of artificial defects, *Phys. Rev. Lett.* **74** 3269-3272.
3. Martín, J. I. *et al.* (1997) Flux pinning in a superconductor by an array of submicrometer magnetic dots, *Phys. Rev. Lett.* **79** 1929-1932.
4. Morgan, D. J. and Ketterson, J. B. (1998) Asymmetric flux pinning in a regular array of magnetic dipoles, *Phys. Rev. Lett.* **80** 3614-3617.
5. Van Bael, M. J. *et al.* (2000) Flux pinning by regular arrays of ferromagnetic dots, *Physica C* **332** 12-19.
6. Van Bael, M. J. *et al.* (1999) Magnetic properties of submicron Co islands and their use as artificial pinning centers, *Phys. Rev. B* **59** 14674-14679.
7. Van Bael, M. J. *et al.* (2001) Local observation of field polarity dependent flux pinning by magnetic dipoles, *Phys. Rev. Lett.* **86** 155-158.
8. Zeper, W. B. *et al.* (1989) Perpendicular magnetic anisotropy and magneto-optical Kerr effect of vapor-deposited Co/Pt-layered structures, *J. Appl. Phys.* **65** 4971-4975.